Semianalytic theory of self-similar optical propagation and mode locking using a shape-adaptive model pulse

Christian Jirauschek[*]

Institute for Nanoelectronics, Technische Universität München, Arcisstraße 21, D-80333 Munich, Germany

F. Ömer Ilday

Department of Physics, Bilkent University, Cankaya, Ankara 06800, Turkey

A semianalytic theory for the pulse dynamics in similariton amplifiers and lasers is presented, based on a model pulse with adaptive shape. By changing a single parameter, this test function can be continuously tweaked between a pure Gaussian and a pure parabolic profile and can even represent sech-like pulses, the shape of a soliton. This approach allows us to describe the pulse evolution in the self-similar and other regimes of optical propagation. Employing the method of moments, the evolution equations for the characteristic pulse parameters are derived from the governing nonlinear Schrödinger or Ginzburg-Landau equation. Due to its greatly reduced complexity, this description allows for extensive parameter optimization, and can aid intuitive understanding of the dynamics. As an application of this approach, we model a soliton-similariton laser and validate the results against numerical simulations. This constitutes a semianalytic model of the soliton-similariton laser. Due to the versatility of the model pulse, it can also prove useful in other application areas.

PACS number(s): 42.65.Tg, 42.65.Sf, 42.55.Wd, 42.65.Re

I. INTRODUCTION

Self-similarity is a recurring theme in strongly nonlinear systems. Its observation can be particularly informative as it implies an underlying symmetry, which can be exploited mathematically through symmetry reduction techniques [1]. In nonlinear optics, self-similarity emerges in the formation of Cantor-set fractals in materials that support spatial solitons [2], the self collapse of beams at high powers, [3] and in the propagation of ultrafast pulses of light in optical fiber amplifiers in the presence of strong Kerr nonlinearity [4,5]. In recent years, it was reported that self-similar propagation of short pulses in laser resonators is possible [6,7]. These pulses have a nearly parabolic intensity profile and evolve self-similarly within the nonlinear segments of the laser cavity. Fiber lasers supporting self-similarly evolving pulses are now recognized as a regime of pulse formation in the cavity of an ultrafast laser. This method is differentiated from the well-known solitary [8], stretched-pulse (dispersion-managed) [9], and all-normal-dispersion [10] solutions to the Haus Master equation [11]. There are interesting similarities as well as important differences between these regimes. From a practical point of view, the demonstration of the similariton laser has led to the development of fiber lasers with significantly higher pulse energies [12]. These fiber lasers are being studied by many groups [13–16], motivated by the various applications ultrafast lasers have in diverse areas of physics, from optical frequency metrology and material processing to next-generation accelerators. More recently, a mode-locking regime, the soliton-similariton laser, was reported, in which the pulse evolution is in the form of periodic alteration between soliton and similariton evolution [17]. One aspect of this regime is that the evolution is strongly nonlinear at every point in the laser cavity. The possibilities and limitations of this

regime are largely in need of exploration, for which theoretical modeling is crucial. For all of these reasons, there is much desire to better understand the physics of amplifier similaritons and self-similar lasers.

Numerical simulations provide good agreement with experiments [6,14,17]. However, they are computationally expensive, rendering extended explorations of the parameter space impractical. Moreover, a theoretical description can aid intuitive understanding of the dynamics of self-similar evolution in optical amplifiers and lasers. Exact self-similar solutions have been derived for the optical pulse propagation in fibers with and without gain [4,5,18]. However, the pulse shape evolves during propagation and the self-similar parabolic pulse profile is only asymptotically reached. Thus, several approaches have been explored to derive a simplified description which still captures the rich pulse dynamics in such systems. Based on various analytical methods, the pulse formation, pulse stability, and energy scalability of similariton and other high-energy fiber lasers has been studied [19–21]. Also semianalytic approaches, widely used in optics to investigate pulse propagation, have been employed. They aim to extract evolution equations for characteristic pulse parameters, reducing the partial differential equation for pulse propagation to a coupled set of ordinary differential equations. Such approaches are typically based on the method of moments (MOM) or a variational formalism, which have both been used to investigate the evolution of the pulse energy and the temporal and spectral pulse width in the strongly nonlinear regime [22–24]. Such studies typically rely on fixed pulse shapes such as Gaussian or sech pulses, yielding reasonable estimates for the pulse energy and duration, but no pulse shape information at all. An exception can be found in [25], where an adaptive super-Gaussian test function was used to investigate changes of the pulse profile during propagation.

Here, we report on a semianalytic theory for the pulse dynamics in similariton amplifiers and lasers, including the soliton-similariton laser, based on a model pulse with adaptive

---

[*]jirauschek@mytum.de

shape. The key in this formulation is our ansatz function that can describe any pulse shape from a pure Gaussian to a pure parabolic profile, including sech-like pulses (i.e., with sech^2 intensity profile), the shape of a soliton. The pulse profile is tweaked by a single parameter, which is complemented by an additional degree of freedom for the pulse phase. This allows us to represent various pulse profiles as well as complex spectral shapes. Thus, our theoretical treatment appears to be capable of describing not only the self-similar but the other regimes as well, opening the way to a simple unified theoretical approach.

Employing the method of moments [26,27], the partial differential equation governing the pulse propagation is reduced to a finite set of coupled ordinary differential equations, which are much easier to analyze. In addition, the coefficients of the equations are helpful in forming an intuitive understanding of the dynamics by exposing the relative importance of the various effects. Through investigation of these equations, one gains access to valuable information about the pulse dynamics (e.g., of how exactly the various effects on the pulse are paired to balance each other to satisfy the periodic boundary conditions imposed by the laser resonator). Such information is extremely difficult, if not impossible, to obtain by repeated numerical solutions of the full governing equation. Our approach is validated against numerical results for single-pass propagation and for the steady-state dynamics of a soliton-similariton laser.

II. TEST PULSE AND EVOLUTION EQUATIONS

For propagation through a dispersive Kerr medium with a parabolic gain and instantaneously saturable absorption, the evolution of the pulse envelope $u(z,t)$ is described by a generalized nonlinear Schrödinger (or complex Ginzburg-Landau) equation of the form [28]

$$i\partial_z u - D\partial_t^2 u + \gamma |u|^2 u = i\left(g + g_\omega \partial_t^2 + r|u|^2\right)u. \quad (1)$$

Here, z and t are the propagation coordinate and the retarded time, respectively. D is the second-order dispersion coefficient, and γ is the cubic nonlinearity parameter. The dissipative processes are characterized by the central gain value g and spectral gain parameter g_ω as well as the saturable absorption coefficient r. Generally, D, γ, g, g_ω, and r are z dependent, since an optical system such as a fiber laser consists of a sequence of different segments. Additionally, the parameter values can vary even within a segment, for example, g, if gain saturation is considered.

A. Test Pulse

For linear systems, $\gamma = r = 0$, the complex Gaussian

$$u(z,\tau) = A\sqrt{p_1(\tau)} \exp(i\beta\tau^2 + i\phi) \quad (2)$$

with $p_1(\tau) = \exp(-\tau^2)$ is an exact solution to Eq. (1), where $\tau = t/T$ denotes the normalized time, and $T(z)$, $A(z)$, $\phi(z)$, and $\beta(z)$ are the pulse duration, amplitude, phase, and linear chirp parameter, respectively. Thus, for moderate nonlinearity, the Gaussian ansatz is still a good description of the

steady-state pulse shape in a laser cavity [29–31]. In contrast, in the strongly nonlinear limit, the pulse is approximately described by a self-similar pulse with a parabolic intensity profile. However, an exactly parabolic pulse is an idealization and in practice the pulse shape is parabolic around the center, where most of the energy resides, but with a super-Gaussian falloff in the wings [6,18]. Naturally, in the intermediate regime, the pulse shape combines features of a Gaussian pulse and a self-similar pulse. To reflect these properties, we have previously introduced a function of the type

$$p_n(\tau) = \exp\left(-\sum_{k=1}^n \tau^{2k}/k\right) = 1 - \tau^2 + O(\tau^{2n+2}) \quad (3)$$

to describe the pulse profile, which represents a Gaussian for $n = 1$ and a parabolic profile for $n \to \infty$ [32]. Here, the pulse duration T represents the Gaussian pulse width for $n = 1$ and half the total pulse width of a similariton for $n \to \infty$. This ansatz has been shown to be useful for the description of similariton lasers and trapped Bose-Einstein condensates [32,33].

A disadvantage of Eq. (3) is that the pulse shape cannot be adapted continuously, but only in discrete steps. Using the Gauss hypergeometric function $_2F_1$ for which efficient numerical evaluation routines exist [34], Eq. (3) can be expressed in closed form as

$$p_n(\tau) = (1 - \tau^2)\exp\left\{\frac{|\tau|^{2n}}{n}[_2F_1(1,n;1+n;\tau^2) - 1]\right\} \quad (4)$$

(see also Appendix A). In Eq. (4), n is not restricted to integers, providing much more flexibility for describing different pulse shapes. For example, sech^2-like intensity profiles, corresponding to a fundamental optical soliton, are very well represented by $n \approx 0.5$. Moreover, rather than *a priori* fixing n to a certain value, we allow $n = n(z)$ to evolve during pulse propagation, describing the position-dependent intensity profile together with the parameters $A(z)$ and $T(z)$. Along with $n(z)$, the third-order chirp parameter $\alpha(z)$ is introduced as a further degree of freedom for the pulse phase in addition to $\beta(z)$ and $\phi(z)$, to avoid mathematical problems with the evolution equations for the pulse parameters [35]. The resulting ansatz for the envelope is given by

$$u(z,\tau) = A\sqrt{p_n(\tau)} \exp(i\beta\tau^2 + i\alpha\tau^4 + i\phi). \quad (5)$$

Naturally, Eq. (4) is not the only function that is able to interpolate continuously between a parabolic and a Gaussian shape. In particular, the so-called q Gaussian function [36] has been used in various contexts (e.g., for the description of trapped Bose-Einstein condensates) [37]. While the q Gaussian has a somewhat simpler analytical form, it is nonzero only on a finite interval (except for the limiting case of a Gaussian), which is unphysical for the applications considered in this paper. Additionally, our ansatz has the distinct advantage that it can also represent a sech^2 profile to a very good approximation, which is essential for a versatile description of nonlinear optical propagation.

B. Evolution Equations

The generalized nonlinear Schrödinger Eq. (1) can be approximately solved by extracting evolution equations for the parameters of the model pulse in Eq. (5). Here we use the method of moments [26]; the derivation can be found in Appendix B. The resulting equations of motion are

$$n' = \left\{ 2rA^2 \left(\frac{\mu_4}{\varepsilon_4} - 2\frac{\mu_2}{\varepsilon_2} + \frac{\mu_0}{\varepsilon_0} \right) + 32\alpha DT^{-2} \left(\frac{\varepsilon_4}{\varepsilon_2} - \frac{\varepsilon_6}{\varepsilon_4} \right) - g_\omega T^{-2} \left[\frac{1}{2}\frac{\eta_0}{\varepsilon_0} - \frac{\eta_2}{\varepsilon_2} + 4\frac{\varepsilon_0}{\varepsilon_2} + \frac{1}{2}\frac{\eta_4}{\varepsilon_4} - 12\frac{\varepsilon_2}{\varepsilon_4} \right.\right.$$
$$\left.+ 8\beta^2 \left(\frac{\varepsilon_2}{\varepsilon_0} - 2\frac{\varepsilon_4}{\varepsilon_2} + \frac{\varepsilon_6}{\varepsilon_4} \right) + 32\alpha^2 \left(\frac{\varepsilon_6}{\varepsilon_0} - 2\frac{\varepsilon_8}{\varepsilon_2} + \frac{\varepsilon_{10}}{\varepsilon_4} \right) + 32\beta\alpha \left(\frac{\varepsilon_4}{\varepsilon_0} - 2\frac{\varepsilon_6}{\varepsilon_2} + \frac{\varepsilon_8}{\varepsilon_4} \right) \right] \right\}$$
$$\bigg/ \left(\frac{\partial_n\varepsilon_0}{\varepsilon_0} - 2\frac{\partial_n\varepsilon_2}{\varepsilon_2} + \frac{\partial_n\varepsilon_4}{\varepsilon_4} \right), \tag{6}$$

$$\frac{T'}{T} = -4DT^{-2} \left(\beta + 2\alpha\frac{\varepsilon_4}{\varepsilon_2} \right) + rA^2 \left(\frac{\mu_2}{\varepsilon_2} - \frac{\mu_0}{\varepsilon_0} \right) + g_\omega T^{-2} \left[\frac{1}{4}\frac{\eta_0}{\varepsilon_0} - \frac{1}{4}\frac{\eta_2}{\varepsilon_2} + \frac{\varepsilon_0}{\varepsilon_2} + 4\beta^2 \left(\frac{\varepsilon_2}{\varepsilon_0} - \frac{\varepsilon_4}{\varepsilon_2} \right) \right.$$
$$\left.+ 16\alpha^2 \left(\frac{\varepsilon_6}{\varepsilon_0} - \frac{\varepsilon_8}{\varepsilon_2} \right) + 16\beta\alpha \left(\frac{\varepsilon_4}{\varepsilon_0} - \frac{\varepsilon_6}{\varepsilon_2} \right) \right] + \frac{1}{2}n' \left(\frac{\partial_n\varepsilon_0}{\varepsilon_0} - \frac{\partial_n\varepsilon_2}{\varepsilon_2} \right), \tag{7}$$

$$\frac{A'}{A} = 2DT^{-2} \left(\beta + 2\alpha\frac{\varepsilon_4}{\varepsilon_2} \right) + g + \frac{1}{2}rA^2 \left(3\frac{\mu_0}{\varepsilon_0} - \frac{\mu_2}{\varepsilon_2} \right) + g_\omega T^{-2} \left[-\frac{3}{8}\frac{\eta_0}{\varepsilon_0} + \frac{1}{8}\frac{\eta_2}{\varepsilon_2} - \frac{1}{2}\frac{\varepsilon_0}{\varepsilon_2} + 2\beta^2 \left(\frac{\varepsilon_4}{\varepsilon_2} - 3\frac{\varepsilon_2}{\varepsilon_0} \right) \right.$$
$$\left.+ 8\alpha^2 \left(\frac{\varepsilon_8}{\varepsilon_2} - 3\frac{\varepsilon_6}{\varepsilon_0} \right) + 8\beta\alpha \left(\frac{\varepsilon_6}{\varepsilon_2} - 3\frac{\varepsilon_4}{\varepsilon_0} \right) \right] + \frac{1}{4}n' \left(\frac{\partial_n\varepsilon_2}{\varepsilon_2} - 3\frac{\partial_n\varepsilon_0}{\varepsilon_0} \right), \tag{8}$$

$$\alpha' = 4\frac{T'}{T}\alpha + \left\{ 2g\alpha\varepsilon_6 + 2rA^2\alpha\mu_6 + \frac{1}{2}g_\omega T^{-2} \left[\beta \left(9\varepsilon_2 - \frac{\varepsilon_0\varepsilon_4}{\varepsilon_2} + \frac{\eta_2\varepsilon_4}{\varepsilon_2} - \eta_4 \right) + \alpha \left(102\varepsilon_4 + 2\frac{\eta_4\varepsilon_4}{\varepsilon_2} - 3\eta_6 - 18\varepsilon_4 \right) \right.\right.$$
$$\left.- 16\beta^2\alpha\varepsilon_8 - 64\beta\alpha^2\varepsilon_{10} - 64\alpha^3\varepsilon_{12} \right] - \alpha\varepsilon_6 \left(2\frac{A'}{A} + 7\frac{T'}{T} \right) - \alpha n'\partial_n\varepsilon_6 - DT^{-2} \left[-\frac{3}{4}\varepsilon_0 + \frac{3}{8}\eta_2 - \frac{1}{8}\frac{\varepsilon_4}{\varepsilon_2}\eta_0 \right.$$
$$\left.\left.+ 8\beta\alpha \left(\varepsilon_6 + 2\frac{\varepsilon_4^2}{\varepsilon_2} \right) + 24\alpha^2 \left(\varepsilon_8 + \frac{\varepsilon_6\varepsilon_4}{\varepsilon_2} \right) \right] - \frac{\gamma}{8}A^2 \left(3\mu_2 - \frac{\mu_0\varepsilon_4}{\varepsilon_2} \right) \right\} \bigg/ \left(\varepsilon_6 - \frac{\varepsilon_4^2}{\varepsilon_2} \right), \tag{9}$$

$$\beta' = 2\frac{T'}{T}\beta - DT^{-2} \left(\frac{1}{4}\frac{\eta_0}{\varepsilon_2} - 4\beta^2 - 48\alpha^2\frac{\varepsilon_6}{\varepsilon_2} - 32\alpha\beta\frac{\varepsilon_4}{\varepsilon_2} \right) - \frac{\gamma}{4}A^2\frac{\mu_0}{\varepsilon_2} + g_\omega T^{-2} \left(\beta\frac{\varepsilon_0}{\varepsilon_2} - \beta\frac{\eta_2}{\varepsilon_2} + 18\alpha - 2\alpha\frac{\eta_4}{\varepsilon_2} \right)$$
$$- 2\frac{\varepsilon_4}{\varepsilon_2} \left(\alpha' - 4\frac{T'}{T}\alpha \right), \tag{10}$$

where the prime denotes a partial derivative with respect to z. The weighing coefficients are given by

$$\varepsilon_k(n) = \int_{-\infty}^{\infty} \tau^k p_n(\tau)\, d\tau,$$
$$\mu_k(n) = \int_{-\infty}^{\infty} \tau^k p_n^2(\tau)\, d\tau, \tag{11}$$
$$\eta_k(n) = \int_{-\infty}^{\infty} \tau^k p_n(\tau)^{-1}[\partial_\tau p_n(\tau)]^2\, d\tau.$$

To increase numerical efficiency, they are calculated only once for a sufficiently closely spaced n grid and tabulated. The evolution equations Eqs. (6)–(10) are also valid for z-dependent coefficients in Eq. (1), which is especially important for effects like gain saturation. We note that the validity of the derived equations is not restricted to ansatz Eq. (4), in fact, they can be used for any such test pulse p_n with a continuously adjustable pulse shape parameter n [and $p_n(\tau) = p_n(-\tau)$], like the q Gaussian function [36,37]. Only the weighing coefficients $\varepsilon_k(n)$, $\mu_k(n)$, and $\eta_k(n)$ [Eq. (11)] then have to be recalculated for that specific function.

III. RESULTS

To validate the ansatz Eq. (5), the equations of motion Eqs. (6)–(10) are solved in different nonlinear propagation regimes. First, the soliton regime is considered, characterized by negative dispersion and moderate nonlinearity. Then, the self-similar propagation through gain fibers with positive dispersion is studied. Finally, the ansatz is employed to find the steady-state solution of a soliton-similariton fiber laser, where alternate propagation in both regimes occurs. The equations of motion Eqs. (6)–(10) are solved with a standard differential equation solver, allowing for an efficient treatment of the problem. For comparison, the results for the simplified Gaussian ansatz Eq. (2) are also shown. The corresponding equations of motion [31] can be obtained from Eqs. (7), (8), and (10) by setting $n = 1$, $\alpha = 0$, and $n' = \alpha' = 0$. The
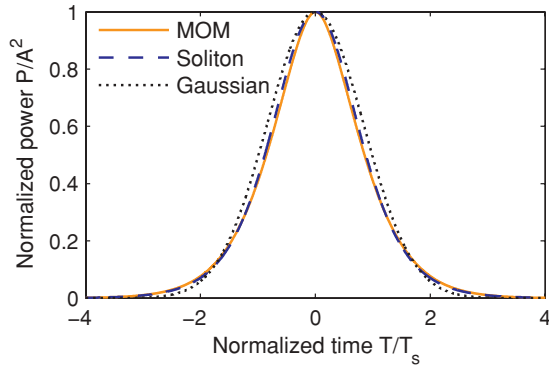
FIG. 1. (Color online) Instantaneous power vs time for the approximate and exact fundamental soliton solution; for comparison, the Gaussian approximation is also displayed.

semianalytic results are validated against exact analytical solutions of Eq. (1) or full numerical simulations performed with a standard symmetric split-step propagation algorithm [28].

A. Fundamental Soliton

For $g = g_\omega = r = 0$, steady-state solutions of Eq. (1) exist. For $\gamma > 0$, $D < 0$ (or $\gamma < 0$, $D > 0$), a special solution is given in form of the fundamental soliton, with the power $|u|^2 = A^2 \text{sech}^2(t/T_s)$, where $T_s = A^{-1}(-2D/\gamma)^{1/2}$ [28]. To test the validity of our ansatz Eq. (5), we extract the steady-state solution of the evolution equations Eqs. (6)–(10) with $g = g_\omega = r = 0$, and compare it to the exact soliton solution. By setting $\partial_z = 0$, we obtain $\beta = \alpha = 0$, $\mu_2\eta_0 + 2\varepsilon_0\mu_0 - \eta_2\mu_0 = 0$, which is fulfilled for $n \approx 0.518$, and $\mu_0\gamma A^2 T^2 = -\eta_0 D$. The pulse energy $E = A^2 T\varepsilon_0$ can thus be written as $E = \varepsilon_0(\eta_0/\mu_0)^{1/2}A(-D/\gamma)^{1/2} \approx 2.79\, A(-D/\gamma)^{1/2}$. The energy of the exact solution of Eq. (1) (i.e., the fundamental soliton) is $E_s = 2^{3/2}A(-D/\gamma)^{1/2}$, thus we have $E \approx 0.99E_s$. The Gaussian ansatz, Eq. (2), is less accurate, yielding $E \approx 1.05E_s$. In Fig. 1, the approximate (solid line) and exact (dashed line) solution are compared for a fixed pulse amplitude A. The results are virtually indistinguishable, demonstrating that the ansatz Eq. (5) works very well in the soliton regime. For comparison, the Gaussian steady-state solution is also displayed (dotted line). It provides a less accurate but still reasonable fit, even though it naturally fails to reproduce the characteristic sech^2 soliton shape.

B. Amplifier Similariton

In order to test our ansatz in the self-similar regime, single-pass propagation in a gain fiber with positive dispersion is studied. The investigated setup is as described in [4], with the fiber parameter values $\gamma = 5.8 \times 10^{-3}\ \text{W}^{-1}\,\text{m}^{-1}$, $D = 12.5 \times 10^{-1}\ \text{ps}^2\,\text{m}^{-1}$, and $g = 0.95\ \text{m}^{-1}$; furthermore, $r = g_\omega = 0$. The initial pulse is assumed to be Gaussian ($n = 1$) with a fixed energy of 12 pJ. First, the pulse evolution is studied with ansatz Eq. (5) and by full numerical simulation for an initial pulse duration of 0.2 ps. Here, the pulse is characterized in terms of its temporal and spectral width T_{FWHM} and f_{FWHM}, respectively, which are the full width at half-maximum (FWHM) values of the instantaneous power and the power spectrum. Furthermore, $n(z)$ is evaluated, describing the pulse shape of our ansatz Eq. (5). For the
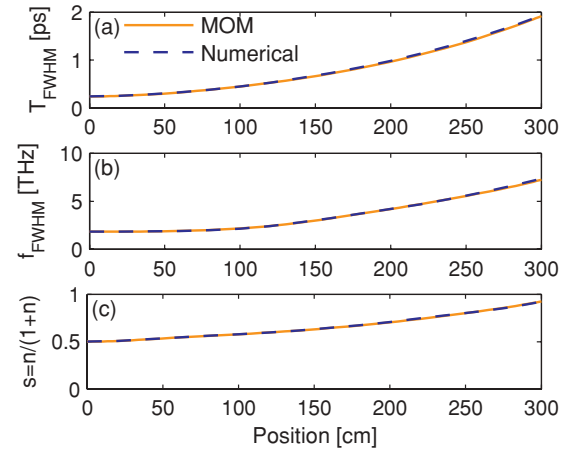

FIG. 2. (Color online) Evolution of the pulse duration, spectral width, and pulse shape as a function of the propagation coordinate z, computed with the method of moments and by solving Eq. (1) numerically.

numerical pulse, the kurtosis [14,25] $\int(t - t_0)^4 p\, dt/\sigma^4$ is calculated, where $p = P/\int P\, dt$ is the normalized pulse power, $t_0 = \int t p\, dt = 0$ is the mean value, and $\sigma^2 = \int(t - t_0)^2 p\, dt$ is the variance; n is then extracted by determining the p_n in Eq. (4) with the same kurtosis. In Fig. 2, the evolution of the pulse parameters is compared for the method of moments and full numerical simulation. In Fig. 2(c), $s = n/(n + 1)$, rather than n itself, is plotted to restrict the range of values to [0,1] (i.e., $s = 1/2$ corresponds to a Gaussian and $s = 1$ to a parabolic pulse). In the example shown, s approaches 1, indicating that the pulse approaches self-similar evolution. The overall agreement between semianalytic and numerical results is excellent, indicating that our approach works well also in the regime of self-similar propagation. Specifically, our ansatz Eq. (5) fully captures the transition of the pulse shape [see Fig. 2(c)].

In Fig. 3, the instantaneous power and power spectrum are shown after a propagation distance of 3 m for Gaussian initial pulse widths (FWHM) of 0.1 ps [Figs. 3(a) and 3(b)], 0.2 ps [Figs. 3(c) and 3(d)], and 1 ps [Figs. 3(e) and 3(f)], respectively. Ansatz Eq. (5) (solid lines) provides an excellent qualitative and quantitative approximation, reproducing very well the exact numerical pulse shapes and power spectra (dashed lines). The Gaussian approach (dotted lines) shows some deviations in the pulse duration and especially the amplitude, but overall still provides a reasonable fit in time domain [see Figs. 3(a), 3(c), and 3(e)]. However, it naturally fails to reproduce the pulse shapes. The Gaussian ansatz does not approximate the pulse shape well, especially for strongly self-similar propagation as shown in Fig. 3(c), where both our ansatz and the exact result exhibit a distinct parabolic intensity profile. Regarding the obtained power spectra [see Figs. 3(b), 3(d), and 3(f)] the Gaussian ansatz completely fails to reproduce the spectral features. The capability to faithfully reproduce spectral characteristics is particularly important from a practical point of view: Experimentally, optical spectra provide the most direct, immediately available, and quite informative insight into the evolution of an ultrafast pulse among all the diagnostics available.
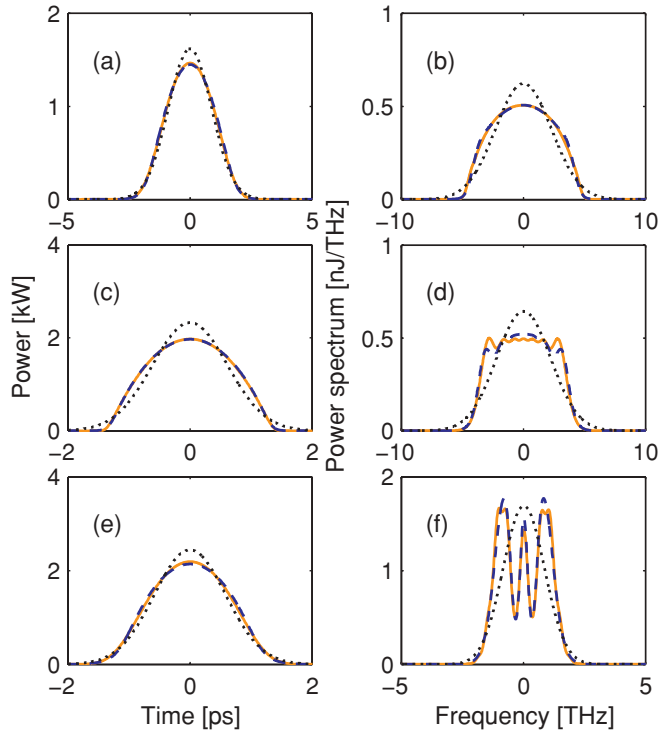
FIG. 3. (Color online) Instantaneous power and power spectrum, as obtained with the method of moments (solid lines), by full numerical simulations (dashed lines), and with the simplified Gaussian ansatz (dotted lines). The initial pulse durations are 0.1, 0.2, and 1 ps, respectively.

C. Soliton-Similariton Fiber Laser

In the following, we apply our approach to self-similar propagation in a laser cavity, where the laser field is subject to periodic boundary conditions in steady-state operation. We choose a soliton-similariton laser setup as investigated in Ref. [17], which is especially interesting in our context since the pulse undergoes self-similar propagation as well as reshaping to Gaussian and sech^2 profiles in the same cavity. In our case, the setup consists of a gain fiber, a piece of single mode fiber (SMF), a saturable absorber (SA), a bandpass filter, and, again, an SMF. The pulse evolves self-similarly in the gain fiber and is temporally and spectrally filtered in the SA and bandpass filter, respectively. The group velocity dispersion (GVD) in the SMF is negative, approximately canceling the positive GVD in the gain fiber. Several distinct nonlinear pulse shapes coexist in the cavity. A parabolic profile is obtained toward the end of the the gain fiber, characteristic for self-similar evolution, then the pulse undergoes Gaussian spectral filtering and approaches a sech^2 shape in the SMF, typical for a fundamental soliton.

The parameter values for the gain fiber (SMF) are $\gamma = 9.32 \times 10^{-3} \, \text{W}^{-1} \, \text{m}^{-1}$ ($1.1 \times 10^{-3} \, \text{W}^{-1} \, \text{m}^{-1}$), $D = 0.03845 \, \text{ps}^2 \, \text{m}^{-1}$ ($-0.0114 \, \text{ps}^2 \, \text{m}^{-1}$), $g_0 = 3.45 \, \text{m}^{-1}$ (0), and $g_\omega = 3.25 \times 10^{-4} \, \text{ps}^2 \, \text{m}^{-1}$ (0) [17]. The gain is assumed to saturate with the pulse energy E [i.e., $g = g_0/(1 + E/E_{\text{sat}})$], where $E_{\text{sat}} = 2.21 \, \text{nJ}$ is the saturation energy. The bandpass filter is modeled by a segment of length L with $g_\omega L = 0.015 \, \text{ps}^2$, corresponding to a spectral width of 12 nm (FWHM), and the pulse power is additionally reduced by a factor of 5 to account

for the overall linear loss of the optical cavity elements. For the SA, an unsaturated loss of $q_0 = 0.7$ and a saturation power of $P_{\text{sat}} = 2.13 \, \text{kW}$ is assumed; its implementation is discussed in Appendix C .
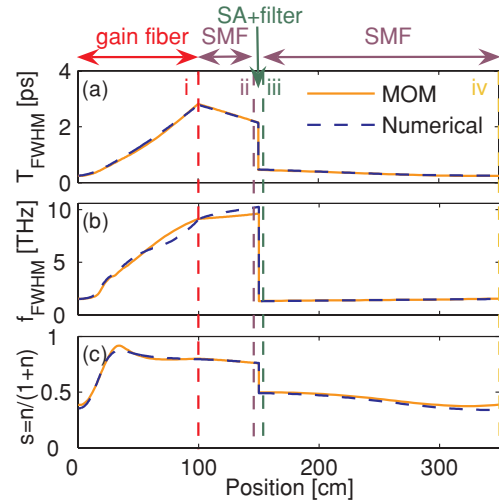

FIG. 4. (Color online) Evolution of the pulse duration, spectral width, and pulse shape in the laser cavity, as obtained with the method of moments and by solving Eq. (1) numerically.
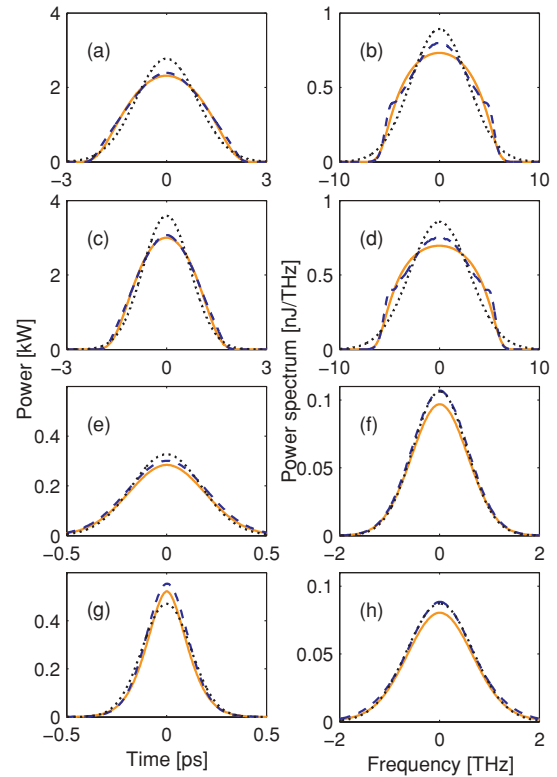

FIG. 5. (Color online) Instantaneous power and power spectrum, as obtained with the method of moments (solid lines), by full numerical simulations (dashed lines), and with the simplified Gaussian ansatz (dotted lines). The results are shown at the positions i(a), i(b), ii(c), ii(d), iii(e), iii(f), iv(g), and iv(h) in the laser cavity, as indicated in Fig. 4(a).

In Fig. 4, the MOM and full numerical results for the evolution of characteristic pulse parameters in the cavity are compared, where the sequence of optical elements and the fiber lengths are as indicated in Fig. 4(a). The pulse parameters are defined as described in Section III B. The overall agreement between semianalytic and numerical results is again excellent (cf. Fig. 2). Particularly, as can be seen in Fig. 4(c), our ansatz Eq. (5) correctly predicts the almost parabolic pulse profile in the gain segment, with $s = 1$ for a parabolic pulse, the Gaussian shape after the filter ($s = 1/2$), as well as the sech^2 shape in the SMF, corresponding to $s \approx 1/3$. In Fig. 5, the instantaneous power and power spectrum are shown after the gain fiber, before the SA, after the bandpass filter, and after the second SMF. The overall agreement between semianalytic (solid lines) and numerical results (dashed lines) is very good both in the gain fiber and the SMF. In particular, ansatz Eq. (5) approximates well the distinct temporal and spectral pulse shapes in the different regimes. For comparison, the Gaussian solution is also displayed (dotted line). It provides a reasonable fit to the temporal and spectral width, but naturally cannot reproduce the pulse shape at all. Only after the bandpass filter, which forces the power spectrum to assume a Gaussian profile, the Gaussian ansatz closely matches the numerical solution [see Fig. 5(f) and 5(h)].

IV. CONCLUSION

In conclusion, we have developed a semianalytic theory for nonlinear optical ultrafast pulse propagation in the self-similar and other regimes, which we employ to study the pulse dynamics in similariton amplifiers and lasers. The key is the introduction of a model pulse with adaptive shape, which can continuously be tweaked with a single parameter to represent pulse shapes ranging from parabolic to Gaussian to sech^2-like intensity profiles. Thus, very different regimes of nonlinear optical propagation can be covered. Based on the method of moments, evolution equations are derived for the characteristic pulse parameters, specifying the pulse amplitude, duration, profile, and linear and third-order chirp. Comparison to exact analytical or full numerical results were performed for the soliton regime as well as similariton amplifiers and soliton-similariton lasers, showing excellent agreement. This constitutes a semianalytic model for the soliton-similariton laser. A major advantage of the semianalytic method is that the calculations are approximately 100 times faster than the full numerical simulations. This will allow the exploration of a vast parameter range of interest to the design of fiber and solid state similariton lasers. Furthermore, this approach can be helpful for developing an intuitive understanding of the dynamics of self-similar evolution in optical fiber systems by exposing the relative importance of the various effects. Due to the versatility of our test function, we expect it to also prove useful in other application areas in nonlinear optics, or in completely different fields such as the description of trapped Bose-Einstein condensates, as already exemplified in Ref. [33].

APPENDIX A: TEST PULSE

The test pulse Eq. (5) can be written as

$$p_n(\tau) = (1 - \tau^2) \exp\left\{ \frac{|\tau|^{2n}}{n} [_2F_1(1,n;1+n;\tau^2) - 1] \right\}$$
$$= (1 - \tau^2) \exp\{|\tau|^{2n}[\Phi(\tau^2,1,n) - n^{-1}]\},$$

where $_2F_1$ is the Gauss hypergeometric function and Φ is the Lerch phi function, defined as $\Phi(z,\alpha,n) = \sum_{k \geqslant 0} z^k/(n+k)^\alpha$ for $|z| < 1$ and analytic continuation otherwise. For $\tau^2 = 1$, where $_2F_1$ and Φ both diverge, p_n has to be expressed in terms of the digamma function $\Psi(z)$ and Euler's constant γ, $p_n(\pm 1) = \exp[-\Psi(n+1) - \gamma]$.

These special functions are routinely implemented in many mathematical tools, and efficient routines are available [34]. However, we found it convenient to evaluate Eq. (5) by a series approach, using

$$p_n(\tau) = (1 - \tau^2) \exp\left(|\tau|^{2n} \sum_{m \geqslant 1} \frac{|\tau|^{2m}}{m+n} \right)$$

for $\tau^2 < 1$ and

$$p_n(\tau) = (\tau^2 - 1) \exp\left(|\tau|^{2n} \sum_{m \geqslant 0} \frac{|\tau|^{-2m}}{m-n} \right) \exp\left\{ \pi \frac{\cos(2\pi n)}{\sin(\pi n)} \right.$$
$$\left. + \pi[2\cos(\pi n) - 1] \tan\left(\frac{3}{2}\pi n \right) \right\}$$

for $\tau^2 > 1$ (and $n \notin \mathbb{N}$). For $n \in \mathbb{N}$, p_n is directly given by Eq. (3).

APPENDIX B: DERIVATION OF THE EQUATIONS OF MOTION

The equations of motion for the pulse parameters are derived using the method of moments [26,27]. We introduce the energy Q_0 and the momentum P_0,

$$Q_0 = \int_{-\infty}^{\infty} |u|^2 dt,$$
$$P_0 = \frac{1}{2} \int_{-\infty}^{\infty} (u_t^* u - u_t u^*)\, dt,$$

and higher-order generalized moments

$$Q_1 = \int_{-\infty}^{\infty} t |u|^2\, dt,$$
$$Q_\ell = \int_{-\infty}^{\infty} (t - t_0)^\ell |u|^2\, dt, \quad \ell > 1$$
$$P_\ell = \int_{-\infty}^{\infty} (t - t_0)^\ell (u_t u^* - u_t^* u)\, dt, \quad \ell > 0$$

where t_0 denotes the center of gravity. Due to the symmetry properties of the ansatz Eq. (5), we have $Q_\ell = 0$ for odd ℓ and $P_\ell = 0$ for even ℓ, as well as $t_0 = 0$.

Multiplying Eq. (1) with u^* and subtracting the complex conjugate, we can write

$$i\partial_z|u|^2 + D\partial_t(u\partial_t u^* - u^*\partial_t u) = u^*R - uR^*, \quad \text{(B1)}$$

with the dissipative term $R = i(g + g_\omega\partial_t^2 + r|u|^2)u$. Multiplying with t^ℓ and integrating over t yields the equations of motion for the Q_ℓ. Furthermore, multiplying Eq. (1) with u_t^* and subtracting u^* times the temporal derivative of Eq. (1), and subsequently taking the real part of the resulting equation yields

$$i\partial_z(u_t^*u - u_tu^*) - 4D\partial_t|u_t|^2 + D\partial_t^3|u|^2 - \gamma\partial_t|u|^4$$
$$= 2(u_tR^* + u_t^*R) - \partial_t(uR^* + u^*R). \quad \text{(B2)}$$

Multiplying with t^ℓ and integrating over t yields the equations of motion for the P_ℓ. We arrive at the evolution equations

$$\partial_z Q_0 = i\int_{-\infty}^{\infty}(uR^* - u^*R)\,dt, \quad \text{(B3)}$$

$$\partial_z Q_2 = 2iDP_1 + i\int_{-\infty}^{\infty}t^2(uR^* - u^*R)\,dt, \quad \text{(B4)}$$

$$i\partial_z Q_4 + 4DP_3 = \int_{-\infty}^{\infty}t^4(u^*R - uR^*)\,dt, \quad \text{(B5)}$$

$$\partial_z P_1 = i\int_{-\infty}^{\infty}(-4D|u_t|^2 - \gamma|u|^4)\,dt + 2i\int_{-\infty}^{\infty}t(u_tR^*$$
$$+ u_t^*R)\,dt + i\int_{-\infty}^{\infty}(uR^* + u^*R)\,dt, \quad \text{(B6)}$$

$$-i\partial_z P_3 + 12D\int_{-\infty}^{\infty}t^2|u_t|^2\,dt - 6DQ_0 + 3\gamma\int_{-\infty}^{\infty}t^2|u|^4\,dt$$
$$= 2\int_{-\infty}^{\infty}t^3(u_tR^* + u_t^*R)\,dt + 3\int_{-\infty}^{\infty}t^2(uR^* + u^*R)\,dt. \quad \text{(B7)}$$

Inserting Eq. (5), we obtain

$$\varepsilon_0\left(2\frac{A'}{A} + \frac{T'}{T}\right) + n'\partial_n\varepsilon_0$$
$$= 2g\varepsilon_0 + 2rA^2\mu_0 + g_\omega T^{-2}$$
$$\times\left(-\frac{1}{2}\eta_0 - 8\beta^2\varepsilon_2 - 32\alpha^2\varepsilon_6 - 32\beta\alpha\varepsilon_4\right), \quad \text{(B8)}$$

$$\varepsilon_2\left(2\frac{A'}{A} + 3\frac{T'}{T}\right) + n'\partial_n\varepsilon_2$$
$$= -8DT^{-2}(\beta\varepsilon_2 + 2\alpha\varepsilon_4) + 2g\varepsilon_2 + 2rA^2\mu_2$$
$$+ 2g_\omega T^{-2}\left(-\frac{1}{4}\eta_2 + \varepsilon_0 - 4\beta^2\varepsilon_4 - 16\alpha^2\varepsilon_8 - 16\beta\alpha\varepsilon_6\right), \quad \text{(B9)}$$

$$\varepsilon_4\left(2\frac{A'}{A} + 5\frac{T'}{T}\right) + n'\partial_n\varepsilon_4 + 16DT^{-2}(\beta\varepsilon_4 + 2\alpha\varepsilon_6)$$
$$= 2g\varepsilon_4 + 2rA^2\mu_4 + g_\omega T^{-2}\left(-\frac{1}{2}\eta_4 + 12\varepsilon_2 - 8\beta^2\varepsilon_6\right.$$
$$\left. - 32\alpha^2\varepsilon_{10} - 32\beta\alpha\varepsilon_8\right), \quad \text{(B10)}$$

$$\left(2\frac{A'}{A} + \frac{T'}{T}\right)(\beta\varepsilon_2 + 2\alpha\varepsilon_4) + \beta'\varepsilon_2 + \beta n'\partial_n\varepsilon_2$$
$$+ 2\alpha'\varepsilon_4 + 2\alpha n'\partial_n\varepsilon_4$$
$$= -DT^{-2}\left(\frac{1}{4}\eta_0 + 4\beta^2\varepsilon_2 + 16\beta\alpha\varepsilon_4 + 16\alpha^2\varepsilon_6\right)$$
$$- \frac{\gamma}{4}A^2\mu_0 + 2g\beta\varepsilon_2 + 4g\alpha\varepsilon_4 + 2rA^2\beta\mu_2$$
$$+ 4rA^2\alpha\mu_4 + g_\omega T^{-2}\left(3\beta\varepsilon_0 - \frac{3}{2}\beta\eta_2 + 42\alpha\varepsilon_2\right.$$
$$\left. - 3\alpha\eta_4 - 48\beta^2\alpha\varepsilon_6 - 96\beta\alpha^2\varepsilon_8 - 8\beta^3\varepsilon_4 - 64\alpha^3\varepsilon_{10}\right), \quad \text{(B11)}$$

$$\left(2\frac{A'}{A} + 3\frac{T'}{T}\right)(\beta\varepsilon_4 + 2\alpha\varepsilon_6) + \beta'\varepsilon_4 + \beta n'\partial_n\varepsilon_4 + 2\alpha'\varepsilon_6$$
$$+ 2\alpha n'\partial_n\varepsilon_6 + \frac{3}{4}\gamma A^2\mu_2 + 3DT^{-2}\left(-\frac{1}{2}\varepsilon_0 + \frac{1}{4}\eta_2\right.$$
$$\left. + 4\beta^2\varepsilon_4 + 16\beta\alpha\varepsilon_6 + 16\alpha^2\varepsilon_8\right)$$
$$= 2g\beta\varepsilon_4 + 4g\alpha\varepsilon_6 + 2rA^2\beta\mu_4 + 4rA^2\alpha\mu_6$$
$$+ g_\omega T^{-2}\left(21\beta\varepsilon_2 - \frac{3}{2}\beta\eta_4 + 102\alpha\varepsilon_4 - 3\alpha\eta_6\right.$$
$$\left. - 48\beta^2\alpha\varepsilon_8 - 96\beta\alpha^2\varepsilon_{10} - 8\beta^3\varepsilon_6 - 64\alpha^3\varepsilon_{12}\right). \quad \text{(B12)}$$

Equation (7) is obtained after multiplying Eq. (B8) by $\varepsilon_2/\varepsilon_0$ and subtracting Eq. (B9); similarly, multiplying Eq. (B8) by $3\varepsilon_2/\varepsilon_0$ and subtracting Eq. (B9) yields Eq. (8). Equation (6) is obtained from Eq. (B10) by inserting Eqs. (7) and (8). Furthermore, we derive Eq. (10) by eliminating $n'\partial_n\varepsilon_2$ and $n'\partial_n\varepsilon_4$ from Eq. (B11), using Eqs. (B9) and (B10), respectively. Finally, Eq. (9) is derived from Eq. (B12) by eliminating $\beta n'\partial_n\varepsilon_4$ with Eq. (B10) and β' with Eq. (10).

APPENDIX C: MODELING OF THE SATURABLE ABSORBER

In the Schrödinger Eq. (1), instantaneously saturable gain or loss is described by the term $\partial_z u|_{\text{sat}} = r|u|^2 u$, with the solution

$$u(L) = \frac{u_0}{\sqrt{1 - 2rL|u_0|^2}} \quad \text{(C1)}$$

for an initial field u_0 and a propagation length L. Thus, the pulse power $P(t) = |u(t)|^2$ is transformed according to

$$P(L) = \frac{P_0}{1 - 2rLP_0}, \quad \text{(C2)}$$

while the phase of u is not altered. For saturable absorption ($r > 0$), this approach only works in the weak field regime (i.e., $2rLP_0 \ll 1$). More generally, a saturable absorber can be modeled by the expression [17]

$$P_1 = P_0\left(1 - \frac{q_0}{1 + P_0/P_{\text{sat}}}\right) = P_0 - q_0P(L), \quad \text{(C3)}$$

where q_0 is the unsaturated loss, and P_{sat} is the saturation power.

In the following, we describe how to obtain the parameter values of our test pulse Eq. (5) after passage through an SA of the form of Eq. (C3). Most straightforwardly, this could be achieved by Taylor expansion of the pulse around its center at the input and output of the SA and comparison of the leading terms [23]. Here, we aim for a more global fitting method, consistent with the MOM. First, the equations of motion Eqs. (6)–(8) are solved for $r = -1/(2P_{\text{sat}}L)$ and $g = g_\omega = D = \gamma = 0$, yielding the pulse parameters $A(L)$, $T(L)$ and $n(L)$ of $P(L)$ in Eq. (C3). The corresponding parameters A_1, T_1, and n_1 for P_1 are then derived by computing the zero, second, and fourth moment of Eq. (C3),

$$\nu_m = \int_{-\infty}^{\infty} t^m P_1 \, dt = \int_{-\infty}^{\infty} t^m P_0 \, dt - q_0 \int_{-\infty}^{\infty} t^m P(L) \, dt \tag{C4}$$

with $m = 0, 2$, and 4, yielding

$$\begin{aligned}\nu_m &= A_0^2 T_0^{m+1}\varepsilon_m(n_0) - q_0 A^2(L) T^{m+1}(L)\varepsilon_m[n(L)] \\ &= A_1^2 T_1^{m+1}\varepsilon_m(n_1),\end{aligned} \tag{C5}$$

with ε_m defined in Eq. (11). From this, we obtain an implicit equation for n_1,

$$\frac{\varepsilon_0(n_1)\varepsilon_4(n_1)}{\varepsilon_2^2(n_1)} = \frac{\nu_0\nu_4}{\nu_2^2}, \tag{C6}$$

and furthermore

$$T_1 = \sqrt{\frac{\varepsilon_0(n_1)\nu_2}{\varepsilon_2(n_1)\nu_0}}, \tag{C7}$$

$$A_1 = \sqrt{\frac{\nu_0}{T_1\varepsilon_0(n_1)}}. \tag{C8}$$

The phase $i\beta(t/T)^2 + i\alpha(t/T)^4 + i\phi$ of our test pulse Eq. (5) is not altered, thus we get $\beta_1 = \beta_0(T_1/T_0)^2$, $\alpha_1 = \alpha_0(T_1/T_0)^4$.

[1] For example, W. F. Ames, *Nonlinear Partial Differential Equations* (Academic, New York, 1967).
[2] M. Soljacic, M. Segev, and C. R. Menyuk, Phys. Rev. E **61**, R1048 (2000).
[3] K. D. Moll, A. L. Gaeta, and G. Fibich, Phys. Rev. Lett. **90**, 203902 (2003).
[4] M. E. Fermann, V. I. Kruglov, B. C. Thomsen, J. M. Dudley, and J. D. Harvey, Phys. Rev. Lett. **84**, 6010 (2000).
[5] V. I. Kruglov, A. C. Peacock, J. M. Dudley, and J. D. Harvey, Opt. Lett. **25**, 1753 (2000).
[6] F. Ö. Ilday, J. R. Buckley, W. G. Clark, and F. W. Wise, Phys. Rev. Lett. **92**, 213902 (2004).
[7] F. Ö. Ilday, F. W. Wise, and F. X. Kärtner, Opt. Express **12**, 2731 (2004).
[8] I. N. Duling III, Electron. Lett. **27**, 544 (1991).
[9] K. Tamura, E. P. Ippen, H. A. Haus, and L. E. Nelson, Opt. Lett. **18**, 1080 (1993).
[10] A. Chong, J. Buckley, W. Renninger, and F. W. Wise, Opt. Express **14**, 10095 (2006).
[11] H. A. Haus, J. G. Fujimoto, and E. P. Ippen, IEEE J. Quantum Electron. **28**, 2086 (1992).
[12] J. R. Buckley, F. W. Wise, F. Ö. Ilday, and T. Sosnowski, Opt. Lett. **30**, 1888 (2005).
[13] C. K. Nielsen *et al.*, Opt. Express **13**, 9346 (2005).
[14] A. Ruehl *et al.*, Opt. Lett. **31**, 2734 (2006).
[15] J. An *et al.*, Opt. Lett. **32**, 2010 (2007).
[16] W. H. Renninger, A. Chong, and F. W. Wise, Phys. Rev. A **82**, 021805 (2010).
[17] B. Oktem, C. Ülgüdür, and F. Ö. Ilday, Nature Photonics **4**, 307 (2010).
[18] D. Anderson *et al.*, J. Opt. Soc. Am. B **10**, 1185 (1993).
[19] B. G. Bale, J. N. Kutz, and F. Wise, Opt. Lett. **33**, 911 (2008).
[20] P.-A. Bélanger, Opt. Express **15**, 11033 (2007).
[21] V. L. Kalashnikov and A. Apolonski, Opt. Express **18**, 25757 (2010).

[22] B. Burgoyne, N. Godbout, and S. Lacroix, Opt. Express **15**, 10075 (2007).
[23] C. Antonelli, J. Chen, and F. X. Kärtner, Opt. Express **15**, 5919 (2007).
[24] B. G. Bale, S. Boscolo, J. N. Kutz, and S. K. Turitsyn, Phys. Rev. A **81**, 033828 (2010).
[25] C.-J. Rosenberg *et al.*, Opt. Commun. **273**, 272 (2007).
[26] A. I. Maimistov, Zh. Eksp. Teor. Fiz. **104**, 3620 (1993) [JETP **77**, 727 (1993)].
[27] E. N. Tsoy, A. Ankiewicz, and N. Akhmediev, Phys. Rev. E **73**, 036621 (2006).
[28] G. P. Agrawal, *Nonlinear Fiber Optics* (Academic, New York, 1989).
[29] Y. Chen *et al.*, J. Opt. Soc. Am. B **16**, 1999 (1999).
[30] C. Jirauschek, F. X. Kärtner, and U. Morgner, J. Opt. Soc. Am. B **20**, 1356 (2003).
[31] C. Jirauschek and F. X. Kärtner, J. Opt. Soc. Am. B **23**, 1776 (2006).
[32] C. Jirauschek, F. Ö. Ilday, and F. X. Kärtner, in *Nonlinear Guided Waves and Their Applications* (Optical Society of America, 2005).
[33] M. Keçeli, F. Ö. Ilday, and M. Ö. Oktel, Phys. Rev. A **75**, 035601 (2007).
[34] W. H. Press, S. A. Teukolsky, W. T. Vetterling, and B. P. Flannery, *Numerical Recipes in C: The Art of Scientific Computing* (Cambridge University Press, New York, 1992).
[35] Without the parameter α (i.e., with three degrees of freedom for the intensity profile but only two for the phase) the method of moments yields terms $\propto \beta^{-1}$ in the equations of motion, causing difficulties for $\beta \to 0$, and the variational method fails completely.
[36] M. Bożejko, B. Kümmerer, and R. Speicher, Commun. Math. Phys. **185**, 129 (1997).
[37] A. I. Nicolin and R. Carretero-González, Physica A **387**, 6032 (2008).